COMMUNICATION

# Electrical Control of Multiferroic Orderings in Mixed-Phase $BiFeO_3$ Films

*Yi-Chun Chen,* Qing He, Feng-Nan Chu, Yen-Chin Huang, Jhih-Wei Chen, Wen-I Liang, Rama K. Vasudevan, Valanoor Nagarajan, Elke Arenholz, Sergei V. Kalinin, and Ying-Hao Chu*

Recent advances in thin-film engineering leads to a new type of mixed-phase system in $BiFeO_3$ (BFO) epitaxial films driven by substrate strain.[1] Single-phase multiferroic BFO had attracted great interests due to its robust ferroelectric and antiferromagnetic orderings at room temperatures.[2–11] Under a strong compressive strain (>4%), the stable crystal structure of BFO transformed from the rhombohedral-like monoclinics (R) to tetragonal-like monoclinics (T),[12,13] and with suitable strain relaxation through thickness, the coexistence of R-BFO and T-BFO phases can be obtained in the same film.[1,14–18] This mixed-phase system can provide a simulated template to reveal origins of unique physical properties in relaxor and morphotropic phase boundary (MPB) materials, such as the large piezoelectric response and the enhanced ferroelectric polarization.[19–22] In addition, recent study showed that in the mixed-phase BFO, the stripe-shape R-BFO embedded in T-BFO matrix possessed nonzero spontaneous magnetic moments along the long axis of the stripe,[23,24] which opens a new direction for strain-driven physics in ferroic oxides.

Creation of T-R phase boundary with controllable ferroic orderings is a critical step towards further mechanism study or novel device realization. It is known that the mixed-phase system can be switched between T- and R-BFO phases by external electric fields.[25,26] However, the formation of ordered mixed-phase structure seems difficult to be obtained, because it involves the selection between many equivalent pathways during the switching history. This problem is similar to that in creating orderly ferroelastic switching in single-phase ferroelectrics, where several local minimum states possessed compatible electrostatic and elastic energies.[27,28] Balke *et al.* had demonstrated successful control of ferroelastic switching in single-phase BFO by breaking the spatial symmetry during the domain nucleation.[29] In mixed-phase BFO, Vasudevan *et al.* had reported the mechanism of T-R transition and created R-BFO phases with specific spatial orientations.[30] However, each orientation of T-R boundary is satisfied with low energy states of two polarization configurations, and the control of them is yet not addressed. Moreover, the interactions between ferroic parameters of the created boundary with those of the matrix are still unknown. In this study, we present an elegant method to systematically create T-R mixed-phase stripes with controllable ferroic boundary conditions by a biased atomic force microscope (AFM) tip, and finally lead to the aim of electrically controllable magnetism. The key factors and mechanisms to break the equivalent variants during T-R phase nucleation are demonstrated, and the fine domain structures at the T-R boundary are also revealed. Besides ferroelectric variants, the ferroelastic orderings of T-R boundaries are controlled by varying the strain-mediated interaction with the T-matrix. In the end, the electrical control of spontaneous magnetic moments in mixed-phase stripes through ordering boundary conditions is presented. This study provides basic understanding to electrically control the unique T-R phase boundary and opens a new route to design strain-mediated magnetoelectric devices.

The resultant phases and domain structures in strained BFO films strongly depend on the poling history (see Supporting information, Figure S1). The topography of as-grown films possessed T-BFO matrix and stripe regions where each stripe valley is the T-R phase boundary.[23] The stripe regions include T and R-BFO phases, and both phases are of domain width about 30 nm, separated by a phase boundary of width about 5 nm, as shown in the TEM images of earlier reports.[1] Detailed domain images in the mixed phase region are shown in Supporting information, Figure S2. It had been reported that the T-matrix in strained BFO is $M_c$ type monoclinic,[12] with in-plane (IP) polarization components mainly parallel to <100> directions. The stabilized domain wall orientations between two adjacent T domains on the surface are along <110> directions.[13] The spatial symmetry for domain nucleation can be broken by the scanning trajectory of the poling tip. Ordered T-BFO domains can be created by the way similar to the control of ferroelastic switching in unstrained single-phase R-BFO.[29] With different combinations of fast and slow

Prof. Y. C. Chen,[+] F. N. Chu, Y.-C. Huang, J. W. Chen
Department of Physics
National Cheng Kung University
Tainan 70101, Taiwan
E-mail: ycchen93@mail.ncku.edu.tw
Dr. Q. He,[+] Dr. E. Arenholz
Advanced Light Source
Lawrence Berkeley National Laboratory
Berkeley, CA 94720, USA
W.-I. Liang, Prof. Y.-H. Chu
Department of Materials Science and Engineering
National Chiao Tung University
Hsinchu 30010, Taiwan
Dr. R. K. Vasudevan, Dr. V. Nagarajan
School of Materials Science and Engineering
University of New South Wales
Sydney, NSW 2052, Australia
Dr. S. V. Kalinin
The Center for Nanophase Materials Sciences
Oak Ridge National Laboratory
Oak Ridge, Tennessee 37831, USA
[+] These authors made equal contributions to this work.

**DOI: 10.1002/adma.201200463**


© 2012 WILEY-VCH Verlag GmbH & Co. KGaA, Weinheim

scanning axes of the biased tip along four IP <110> directions, a total of four kinds of ordered T domain structures can be obtained (see Supporting information, Figure S3). Each stable domain structure of T-matrix includes two domains, and on the boundary between two different T-matrixes, IP polarization components of four adjacent domains can construct a closure vortex. The summarized rule to control the T-BFO domain orderings is that the obtained domain structure has the domain walls parallel to the fast writing axis, and the net IP polarization of two composed T domains is opposite to the direction of the slow writing axis (Figure S3).

Highly-ordered T-R mixed phases and their boundaries can be further controlled through fast-scanning directions of the writing tip. A negative-biased tip was used to write the mixed-phase stripes on a pre-switched downward polarized T-BFO matrix. The poled rectangles in **Figure 1** were obtained by a writing process where the bias was only turned on in one specific direction during the fast-axis scanning, as indicated in Figure 1a and 1g. The orientation of the T-R phase boundary on the surface is mainly along [100] or [010], with the relaxed boundary tails tilting about 10° from the main directions, so most boundaries look like curved stripes (Figure 1c,d,i,j). Our pervious study about the T-R transition mechanism[30] indicated that the created mixed-phase stripes tend to be perpendicular to the writing axis, and the activation energy to nucleate R-BFO is smaller than that to switch out-of-plane (OP) polarization (also see Supporting information, Figure S4). When the writing direction of fast axis was also controlled, the curvature tendency of the stripe became an adjustable ordering parameter. Figure 1a and 1g show that the created stripes curved toward the tip moving direction along <100>. Note that the domain structures in mixed-phase region are closely related to the stripe curving directions. Each curved loop shown in IP PFM images (Figure 1e,f,k,l) is of the T-R phase boundary.[23] One side of the loop coincides with the stripe valley while the other side coincides with the stripe peak in topography. R-BFO phases are circled inside the loops, and T-BFO phases are located between the loops.[23] The IP polarizations of the phase boundaries are mainly perpendicular to the stripe orientations and parallel to <100> directions, as indicated by the arrows in the IP PFM images. Different slopes between upper and lower segments of the same stripe correspond to two different low-energy domain structures. In the as-grown states with downward OP polarization, the IP component at the phase boundary is parallel to the stripe-curving direction, while in the switched region with upward OP polarization, the IP component at the phase boundary is anti-parallel to the stripe-curving direction.

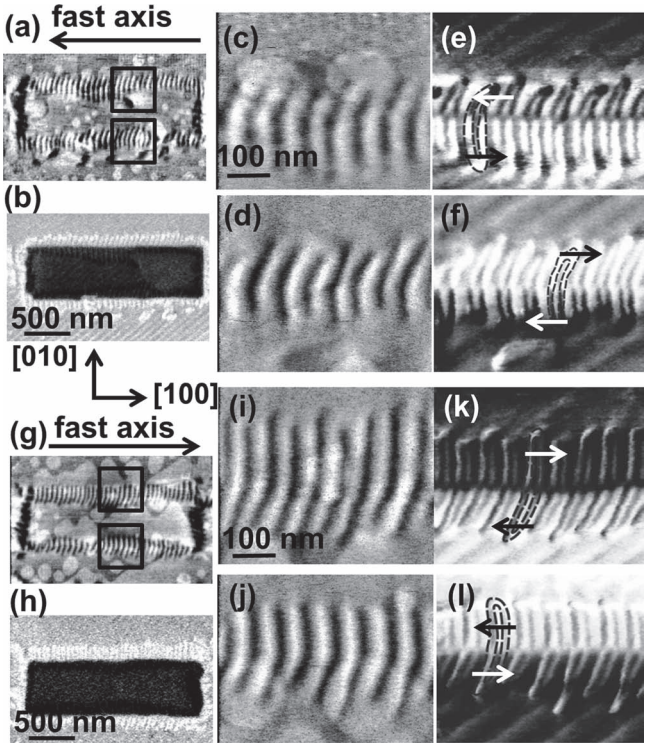


**Figure 1.** a,g) Topography images and b,h) OP PFM images of a rectangle poled by a scanning tip with -10 V tip bias only applied in one fast-axis direction. The arrows above (a,g) indicated the scanning direction of the fast axis where the writing bias was turned on. The bright and dark contrasts in OP PFM correspond to downward and upward OP components, respectively. c,d) The enlarged topography images and e,f) IP PFM images of the squared regions in the upper and lower edges of the switched area in (a), respectively. i,j) The enlarged topography images and k,l) IP PFM images of the squared regions in the upper and lower edges of the switched area in (g), respectively. These images were scanned with the cantilever parallel to [010]. The bright and dark contrasts in IP PFM correspond to rightward and leftward IP components, respectively. The arrows in (e,f,k,l) indicate the IP polarization directions of the T-R phase boundary. Scale bars in (c,d,e,f) and (i,j,k,l) are the same.

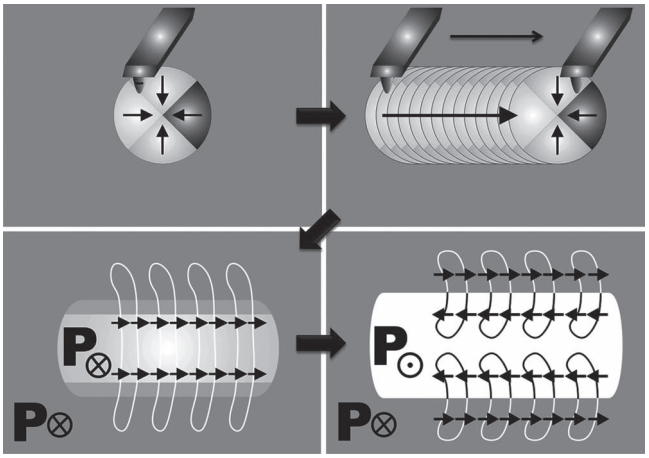


**Figure 2.** Schematics of the formation of ordered mixed-phase stripes on a T-matrix. The IP electric fields at rear parts of the scanning trajectory dominate the polarization directions of resultant domains. The mixed-phase stripes nucleate before OP polarization switching in the poled region. The final stage is the 180° ferroelectric switching of half segments of the stripes.

**Figure 2** illustrates the possible pathway for the formation of ordered mixed-phase stripe on a T-matrix under electric fields from a moving tip. Since the T-R phase boundaries have stronger IP components than adjacent T and R phases, the interaction between the polarization at the phase boundary and external fields breaks the nucleation symmetry. The first


© 2012 WILEY-VCH Verlag GmbH & Co. KGaA, Weinheim

diagram in Figure 2 shows the polarization directions at T-R boundary favored by the IP fields from a negative-biased tip. As mentioned earlier, the IP polarization of the boundary was mainly perpendicular to the orientation of the stripe. Therefore, when the tip was writing along [110] direction, two preferred polarization components, [100] or [010], resulted in two possible stripe orientations. By contrast, when the tip was writing along [100], as shown in Figure 2, only one IP component at the boundary was preferred by the nucleation sequence, i.e. [100], the tip field at the back side of the writing trajectory. Moreover, due to the smaller nucleation energy of R-BFO phases, mixed-phase stripes were formed before OP switching.[30] With downward OP polarization, the T-R boundary with IP component directing to [100] was then stabilized with the shape curving toward positive [100] direction. The formed stripes spilt into two sections when the OP polarization in the middle region was switched upward due to high field stress and transformed to the matrix T-BFO. The resultant domain structures in Figure 1 suggest that the final stage was the 180° ferroelectric switching in half of the mixed-phase region, as illustrated in the last diagram of Figure 2. Without changing the monoclinic distortion axis, the final OP switching didn't involve additional elastic energy. Therefore, the created mixed-phase stripes have the same ferroelastic ordering parameters with the as-grown stripes possessing the same topography.

The tilting of the scanning axis provides another degree of freedom to control the ferroelastic orderings in mixed-phase stripes. As shown in **Figure 3**a, when edges of a poled rectangle tilted away from the [100] direction, the mixed-phase stripes on the rectangle edges transformed from curved to straight geometry. Basically, the straight stripes occurred when the scanning axis was titled from [100] for more than 20°. The topography and domain structures of the straight mixed-phase stripes are shown in Figure 3b–d. Note that the T-R phase boundaries no longer possess domains shaped in closed loops; instead, the IP PFM images show meandering S-shaped boundaries. This result indicates that for the straight mixed-phase stripe, the T-BFO in the OP switched segment was adjacent to the R-BFO phase in the OP un-switched segment. Moreover, unlike the domain structures in curved stripes (Figure 1), the IP polarizations of T-R phase boundary in the OP switched and non-switched segments of a straight stripe were the same. Same IP but opposite OP components reveal that the monoclinic distortion axes of these two segments are different, which results in another type of ferroelastic ordering in the mixed-phase region. The as-grown stripes tended to arrange along [100] or [010] directions; therefore, driving the mixed-phase stripes to align along largely-deviated direction will involve strong elastic interaction. The resultant structure was stabilized by releasing shear strained energy so that the IP monoclinic distortions were tilted in opposite directions on two sides of the boundary created along the writing direction.

The manipulation of T-R phase boundaries with different ferroic orderings is summarily demonstrated in **Figure 4**a. The ferroelectric variants of T-BFO and mixed-phase stripes were controlled by slow scanning axis and fast scanning axis of the poling process, respectively. Therefore, ordered T-BFO matrix and mixed-phase domains can be manipulated independently. Four combinations of the T-BFO matrix domains were obtained,

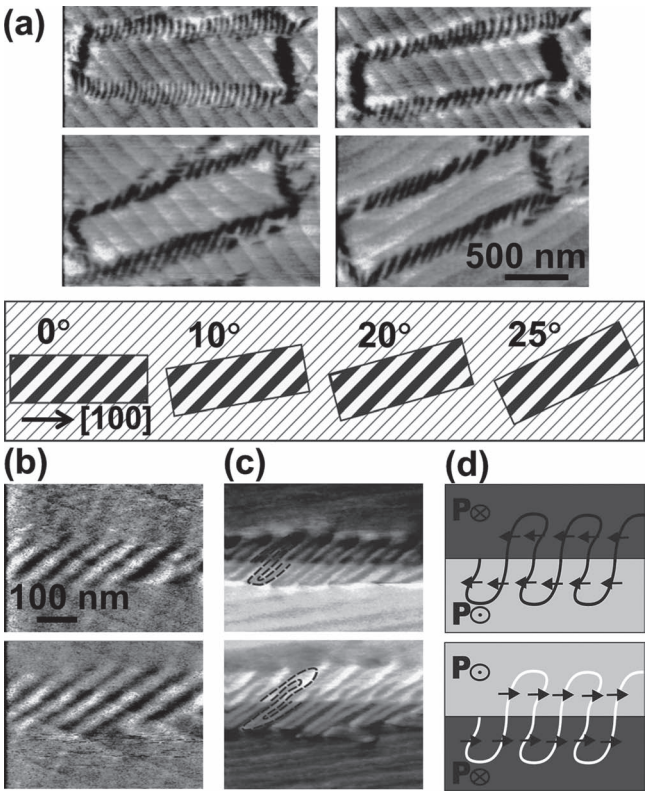


**Figure 3.** a) The topography variation of mixed-phase stripes created by a biased tip with different scanning angle. The stripes became less curved when the scanning angle to [100] direction was increased. The bottom diagram illustrates the relative orientation of the poled edges where mixed-phase stripes were aligned on T-BFO matrixes. b) Topography, c) IP PFM, and d) illustration of domain structures of the mixed phase stripes formed at the upper and lower edges of a poled rectangle, which was written with a scanning angle of 20°. The IP PFM images were scanned with the cantilever parallel to [010]. The arrows in (d) illustrated the IP polarizations at T-R boundaries.

and the mixed-phase stripes were created along the edges of the poled rectangles. The right-up and left-down insets in Figure 4a show the details of two kinds of curved stripes with opposite polarization variants, as discussed earlier, which were also correlated with their stripe-curving directions. The vertically-titled and the horizontally-titled rectangles in Figure 4a were written with the fast axis deviating from [010] for 25° and 10°, respectively. Correspondingly, straight and curved stripes with different ferroelastic ordering parameters were successfully formed on the edges of the vertically-titled and the horizontally-titled rectangles, respectively.

In single-phase BFO thin films with ground-state rhombohedral crystal structure (space group *R3C*), a nonzero weak magnetic moment due to the antiferromagnetic canting is expected,[7] while in strained BFO films, this spontaneous moment is strongly enhanced, forming detectable magnetic domains in the distorted monoclinic R-BFO phases circled by the T-R phase boundaries.[23] The spatial variation of strain has strong gradient near the T-R phase boundary, so the inhomogeneous interaction between the spatially modulated


© 2012 WILEY-VCH Verlag GmbH & Co. KGaA, Weinheim

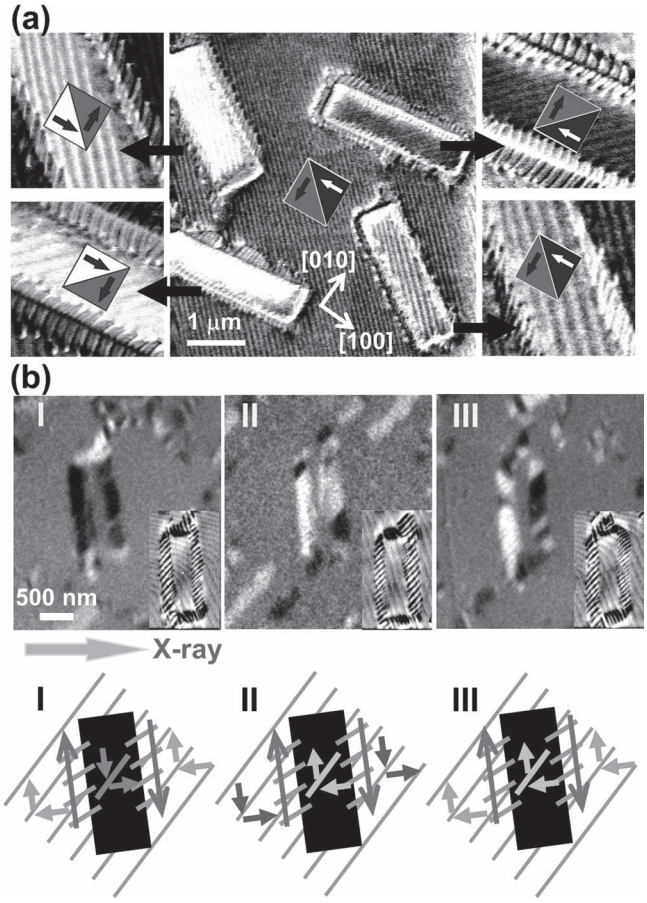


**Figure 4.** a) IP PFM images of ordered mixed-phase domains created at boundaries between two T-BFO matrixes with controlled polarization variants. Four different combinations of T-BFO matrixes, and mixed-phase stripes with different polarization variants and ferroelastic orderings were demonstrated. The insets illustrated the IP polarizations of T-BFO matrixes. The IP-PFM images were scanned with cantilever parallel to [010]. b) XMCD-PEEM images of straight mixed-phase stripes created at boundaries with three different combinations of T-matrix ordering. White and black contrasts indicate magnetic moments parallel and anti-parallel to the incident X-rays. The inset of each image shows the topography and the bottom diagram illustrates the ferroelectric variants. The arrows indicate the IP polarization directions of T-BFO matrixes and T-R boundaries. The dark areas were OP switched upward.

magnetic moments and electric polarizations will play an important role in the magnetoelectric couplings. Therefore, it's crucial to know the magnetic properties in the mixed-phase region with controllable environmental ferroelectric and ferroelastic orderings. Figure 4b shows X-ray magnetic circular dichroism-based photoemission electron microscopy (XMCD-PEEM) images of three mixed-phase regions which were created with straight stripes and different combinations of ordering T-BFO matrixes. The contrasts in XMCD-PEEM images indicate the IP magnetic moments parallel or anti-parallel to the incident X-ray, which show the magnetic moments are located in the R-BFO and parallel to the long axis of the stripes. In Figure 4b, the ferroelectric and ferroelastic orderings in mixed-phase region I and II are symmetric with each other for an operation of 180° rotation about the sample normal; remarkably, the magnetic contrasts of these two mixed-phase stripes are opposite, agreeing with the rotation symmetry. This result indicates that the magnetic moments are controllable by local environmental orderings. Mixed-phase region III has the T-matrix variants same as region I inside the poled rectangle and same as region II outside the poled rectangle. The magnetic contrasts of two mixed-phase stripes in region III are one dark and one bright on each rectangle edge. Note that the ferroelectric and ferroelastic orderings of the straight mixed-phase stripes possess in-plane 180° rotation symmetry while the IP variants of T-matrix are inversed under the 180° rotation. The result that the magnetic orientations of the stripes in region III possessed different IP rotation symmetry from those in region I and II indicates that the magnetic moments are complexly coupling to both ferroelectric and ferroelastic orderings. Some magnetic disorders were also observed, which corresponded to the appearance of random curved stripes due to the relaxation near the rectangular corner.

Two possible mechanisms may cause the dependence of magnetic moments on the environmental ferroelectric orderings. One is the flexomagnetic interaction, where the large strain gradient across the phase boundary induces specific magnetization. When changing the domain structures in the T-matrixes adjacent to the mixed-phase stripes, the monoclinic distortion directions of T-BFO matrixes also vary with their ferroelectric easy axes through the piezoelectric coupling. The spatial variation of strain from the T-matrixes to the R-BFO phases could be responsible for the flexomagnetic interaction. Note that the strain distribution near the phase boundary is more complex than that at the regular domain wall and may be nonlocal. The other possible mechanism is the flexomagnetoelectric interaction. In $BiFeO_3$ thin films, although the spin cycloid is suppressed, theoretical estimation based on the inhomogeneous magnetoelectric interaction suggested the ferroelectric stripe domain structures can also induce the modulation of antiferromagnetic vectors, which possess abrupt magnetization deviations at the ferroelectric domain boundaries.[31] In strained $BiFeO_3$, both the strain and polarization gradients across phase boundaries could be significant. The couplings between magnetization, polarization, and strain in the mixed-phase region cause interesting nano-scale multiferroic properties. Although the detailed mechanism to result in specific magnetic orientation is unclear, based on the preliminary observations, the spontaneous magnetic moments at the T-R boundary are sensitive to local environment ordering parameters and thus electrically controllable. The systematic way provided in this study to create different ordering boundaries is a key step for further investigation.

In summary, a systematic way was demonstrated to create T-R phase boundaries with different ferroic-ordering environments. Ordered mixed-phase stripes were controlled by the writing trajectories of a biased AFM tip. The fast-scanning axis determines the polarization variants of the mixed-phase stripes while the slow-scanning axis governs the ordered domains in T-BFO matrix, so the ferroelectric ordering in matrix and mixed-phase region can be controlled independently. The fine domain


© 2012 WILEY-VCH Verlag GmbH & Co. KGaA, Weinheim

structures in mixed phase region show curving-direction-dependent polarity. When the mixed-phase stripes were electrically driven to form along a scanning axis tilting away from [100] or [010], the additional lateral elastic stress resulted in a new type of ferroelastic orderings. Controllable combinations of ordering parameters in local environment open the new route to design studies on the mechanism of unique physical properties at the T-R phase boundary. XMCD-PEEM images show that spontaneous magnetic moments are correlated with the local ordering parameters. Consequently, manipulation of both ferroelectric and ferroelastic orderings at the T-R phase boundaries provide the possibility to electrically control the magnetic orientations at room temperatures.

## Experimental Section

The mixed-phase $BiFeO_3$ (BFO) films of 150 nm thickness were grown by pulsed laser deposition on the conducting $LaNiO_3$ (LNO) buffered (001) $LaAlO_3$ (LAO) substrates. Surface topography and piezoresponse force microscopy (PFM) images were examined by a commercial scanning probe microscope (CPII, Veeco) equipped with a lock-in amplifier. Commercial Pt-Ir coated tips with elastic constants about 4 N/m were used for applying switching fields and performing PFM measurements. During the domain imaging, an ac voltage of 1.0 V at 6.39 kHz was applied as modulation. The ordered ferroic domains were created by designed poling procedures through the tip as discussed in the results. The writing interval between points on the fast scanning axis is about 4 ms, while the writing interval along the slow scanning axis is the inverse of tip line-scanning rate, which is about 1 s. All IP PFM images shown in this paper were scanned with the cantilever parallel to the [010] direction of the sample.

X-ray magnetic circular dichroism-based photoemission electron microscopy (XMCD-PEEM)[32] was used to examine the spontaneous magnetic moments on the manipulated mixed-phase boundaries. The X-rays were incident on the sample at an angle of 30° from the surface, and the focusing spot is about 30 μm in diameter. The XMCD-PEEM images were measured by tuning the photon energy to the Fe $L_3$-edge (~710 eV), and right- and left- handed circularly polarized (RCP or LCP) radiations were used. The imaging of magnetic moments was performed by taking the ratio between LCP and RCP at every location.

## Supporting Information

Supporting Information is available from the Wiley Online Library or from the author

## Acknowledgements

Y. C. Chen and Y. H. Chu acknowledge the financial support of the National Science Council, R.O.C., through projects NSC 99-2112-M-006-012-MY3 and NSC 100-2119-M-009-003. Q. He and E. Arenholz of the Advanced Light Source are supported by the U.S. Department of Energy under Contract No. DE-AC02-05CH11231. R. K. Vasudevan and V. Nagarajan acknowledge ARC Discovery Project DP1096669. S. V. Kalinin is supported by the Center for Nanophase Materials Sciences at Oak Ridge National Laboratory, which is sponsored by the Office of Basic Energy Sciences, U.S. Department of Energy.

Received: February 2, 2012
Revised: March 21, 2012
Published online: May 9, 2012

[1] R. J. Zeches, M. D. Rossell, J. X. Zhang, A. J. Hatt, Q. He, C. H. Yang, A. Kumar, C. H. Wang, A. Melville, C. Adamo, G. Sheng, Y. H. Chu, J. F. Ihlefeld, R. Erni, C. Ederer, V. Gopalan, L. Q. Chen, D. G. Schlom, N. A. Spaldin, L. W. Martin, R. Ramesh, *Science* **2009**, *326*, 977.
[2] C. Ederer, N. A. Spaldin, *Phys. Rev. Lett.* **2005**, *95*, 257601.
[3] J. Wang, J. B. Neaton, H. Zheng, V. Nagarajan, S. B. Ogale, B. Liu, D. Viehland, V. Vaithyanathan, D. G. Schlom, U. V. Waghmare, N. A. Spaldin, K. M. Rabe, M. Wuttig, R. Ramesh, *Science* **2003**, *299*, 1719.
[4] G. Catalan, J. F. Scott, *Adv. Mater.* **2009**, *21*, 2463.
[5] F. Zavaliche, S. Y. Yang, T. Zhao, Y. H. Chu, M. P. Cruz, C. B. Eom, R. Ramesh, *Phase Transit* **2006**, *79*, 991.
[6] Y. H. Chu, L. W. Martin, M. B. Holcomb, R. Ramesh, *Mater. Today* **2007**, *10*, 16.
[7] C. Ederer, N. A. Spaldin, *Phys. Rev. B* **2005**, *71*, 060401.
[8] T. Zhao, A. Scholl, F. Zavaliche, K. Lee, M. Barry, A. Doran, M. P. Cruz, Y. H. Chu, C. Ederer, N. A. Spaldin, R. R. Das, D. M. Kim, S. H. Baek, C. B. Eom, R. Ramesh, *Nat. Mater.* **2006**, *5*, 823.
[9] Y. H. Chu, L. W. Martin, M. B. Holcomb, M. Gajek, S. J. Han, Q. He, N. Balke, C. H. Yang, D. Lee, W. Hu, Q. Zhan, P. L. Yang, A. Fraile-Rodriguez, A. Scholl, S. X. Wang, R. Ramesh, *Nat. Mater.* **2008**, *7*, 678.
[10] D. Lebeugle, D. Colson, A. Forget, M. Viret, P. Bonville, J. F. Marucco, S. Fusil, *Phys. Rev. B* **2007**, *76*, 024116.
[11] D. Lebeugle, D. Colson, A. Forget, M. Viret, A. M. Bataille, A. Gukasov, *Phys. Rev. Lett.* **2008**, *100*, 227602.
[12] H. M. Christen, J. H. Nam, H. S. Kim, A. J. Hatt, N. A. Spaldin, *Phys. Rev. B* **2011**, *83*, 144107.
[13] Z. H. Chen, Z. L. Luo, Y. J. Qi, P. Yang, S. X. Wu, C. W. Huang, T. Wu, J. L. Wang, C. Gao, T. Sritharan, L. Chen, *Appl. Phys. Lett.* **2010**, *97*, 242903.
[14] Z. H. Chen, S. Prosandeev, Z. L. Luo, W. Ren, Y. J. Qi, C. W. Huang, L. You, C. Gao, I. A. Kornev, T. Wu, J. L. Wang, P. Yang, T. Sritharan, L. Bellaiche, L. Chen, *Phys. Rev. B* **2011**, *84*, 094116.
[15] I. C. Infante, J. Juraszek, S. Fusil, B. Dupe, P. Gemeiner, O. Dieguez, F. Pailloux, S. Jouen, E. Jacquet, G. Geneste, J. Pacaud, J. Iniguez, L. Bellaiche, A. Barthelemy, B. Dkhil, M. Bibes, *Phys. Rev. Lett.* **2011**, *107*, 237601.
[16] Z. H. Chen, L. You, C. W. Huang, Y. J. Qi, J. L. Wang, T. Sritharan, L. Chen, *Appl. Phys. Lett.* **2010**, *96*, 252903.
[17] H.-J. Liu, C.-W. Liang, W.-I. Liang, H.-J. Chen, J.-C. Yang, C.-Y. Peng, G.-F. Wang, F.-N. Chu, Y.-C. Chen, H.-Y. Lee, L. Chang, S.-J. Lin, Y.-H. Chu, *Phys. Rev. B* **2012**, *85*, 014104.
[18] A. R. Damodaran, S. Lee, J. Karthik, S. MacLaren, L. W. Martin, *Phys. Rev. B* **2012**, *85*, 024113.
[19] Y. Y. Liu, J. Y. Li, *Phys. Rev. B* **2011**, *84*, 132104.
[20] H. Y. Kuo, Y. C. Shu, H. Z. Chen, C. J. Hsueh, C. H. Wang, Y. H. Chu, *Appl. Phys. Lett.* **2010**, *97*, 242906.
[21] A. R. Damodaran, C. W. Liang, Q. He, C. Y. Peng, L. Chang, Y. H. Chu, L. W. Martin, *Adv. Mater.* **2011**, *23*, 3170.
[22] J. X. Zhang, Q. He, M. Trassin, W. Luo, D. Yi, M. D. Rossell, P. Yu, L. You, C. H. Wang, C. Y. Kuo, J. T. Heron, Z. Hu, R. J. Zeches, H. J. Lin, A. Tanaka, C. T. Chen, L. H. Tjeng, Y. H. Chu, R. Ramesh, *Phys. Rev. Lett.* **2011**, *107*.
[23] Q. He, Y. H. Chu, J. T. Heron, S. Y. Yang, W. I. Liang, C. Y. Kuo, H. J. Lin, P. Yu, C. W. Liang, R. J. Zeches, W. C. Kuo, J. Y. Juang, C. T. Chen, E. Arenholz, A. Scholl, R. Ramesh, *Nat. Commun.* **2011**, *2*, 225.
[24] K. T. Ko, M. H. Jung, Q. He, J. H. Lee, C. S. Woo, K. Chu, J. Seidel, B. G. Jeon, Y. S. Oh, K. H. Kim, W. I. Liang, H. J. Chen, Y. H. Chu,


© 2012 WILEY-VCH Verlag GmbH & Co. KGaA, Weinheim

Y. H. Jeong, R. Ramesh, J. H. Park, C. H. Yang, *Nat. Commun.* **2011**, *2*, 567.
[25] J. X. Zhang, B. Xiang, Q. He, J. Seidel, R. J. Zeches, P. Yu, S. Y. Yang, C. H. Wang, Y. H. Chu, L. W. Martin, A. M. Minor, R. Ramesh, *Nat. Nanotechnol.* **2011**, *6*, 97.
[26] D. Mazumdar, V. Shelke, M. Iliev, S. Jesse, A. Kumar, S. V. Kalinin, A. P. Baddorf, A. Gupta, *Nano Lett.* **2010**, *10*, 2555.
[27] R. K. Vasudevan, Y. C. Chen, H. H. Tai, N. Balke, P. P. Wu, S. Bhattacharya, L. Q. Chen, Y. H. Chu, I. N. Lin, S. V. Kalinin, V. Nagarajan, *Acs Nano* **2011**, *5*, 879.
[28] Y. C. Chen, G. F. Wang, H. H. Tai, J. W. Chen, Y. C. Huang, J. C. Yang, Y. H. Chu, *Nanotechnology* **2011**, *22*, 254030.
[29] N. Balke, S. Choudhury, S. Jesse, M. Huijben, Y. H. Chu, A. P. Baddorf, L. Q. Chen, R. Ramesh, S. V. Kalinin, *Nat. Nanotechnol.* **2009**, *4*, 868.
[30] R. K. Vasudevan, Y. Y. Liu, J. Y. Li, W. I. Liang, A. Kumar, S. Jesse, Y. C. Chen, Y. H. Chu, V. Nagarajan, S. V. Kalinin, *Nano Lett.* **2011**, *11*, 3346.
[31] A. P. Pyatakov, A. K. Zvezdin, *Eur. Phys. J. B* **2009**, *71*, 419.
[32] F. de Groot, *Chem. Rev.* **2001**, *101*, 1779.


© 2012 WILEY-VCH Verlag GmbH & Co. KGaA, Weinheim